measure of the stability of the collagen-like triple-helical structure.

Acknowledgment. We thank Dr. S. S. Zimmerman for helpful discussions and M. S. Pottle and S. Rumsey for extensive help with the computations. This work was supported by research grants from the National Science Foundation (PCM75-08691) and from the National Institute of General Medical Sciences (GM-14312) and the National Institute on Aging (AG-00322) of the National Institutes of Health.

Miniprint Material Available: Full-size copies of Tables I–VII (7 pages). Ordering information is given on any current masthead page.

References and Notes

(1) Presented before the Division of Cellulose, Paper, and Textile at the 178th National Meeting of the American Chemical Society, Washington, D.C., Sept 1979, Abstract No. CELL 13.
(2) Miller, M. H.; Scheraga, H. A. *J. Polym. Sci., Polym. Symp.* **1976**, *54*, 171.
(3) Miller, M. H.; Némethy, G.; Scheraga, H. A. *Macromolecules* **1980**, *13*, 470.
(4) Miller, M. H.; Némethy, G.; Scheraga, H. A. *Macromolecules* **1980**, *13*, 910.
(5) Traub, W.; Piez, K. A. *Adv. Protein Chem.* **1971**, *25*, 243.
(6) Bhatnagar, R. S.; Rapaka, R. S. In "Biochemistry of Collagen"; Ramachandran, G. N., Reddi, A. K., Eds.; Plenum Press: New York and London, 1976; p 479.
(7) Hulmes, D. J. S.; Miller, A.; Parry, D. A. D.; Piez, K. A.; Woodhead-Galloway, J. *J. Mol. Biol.* **1973**, *79*, 137.
(8) Fietzek, P. P.; Glanville, R. W., personal communication.
(9) Segal, D. M.; Traub, W. *J. Mol. Biol.* **1969**, *43*, 487.
(10) Doyle, B. B.; Traub, W.; Lorenzi, G. P.; Blout, E. R. *Biochemistry* **1971**, *10*, 3052.
(11) Scatturin, A.; Tamburro, A. M.; Del Pra, A.; Bordignon, E. *Int. J. Pept. Protein Res.* **1975**, *7*, 425.
(12) Tamburro, A. M.; Scatturin, A.; Del Pra, A. *Int. J. Pept. Protein Res.* **1977**, *9*, 310.
(13) Momany, F. A.; McGuire, R. F.; Burgess, A. W.; Scheraga, H. A. *J. Phys. Chem.* **1975**, *79*, 2361.
(14) (a) Al-Karaghouli, A. P.; Koetzle, T. F. *Acta Crystallogr., Sect. B* **1975**, *31*, 2461. (b) Power, L. F.; Turner, K. E.; Moore, F. H. *Ibid.* **1976**, *32*, 11. (c) Kvick, Å.; Al-Karaghouli, A. R.; Koetzle, T. F. *Ibid.* **1977**, *33*, 3796.
(15) Zimmerman, S. S.; Scheraga, H. A. *Biopolymers* **1977**, *16*, 811.
(16) Tanaka, S.; Scheraga, H. A. *Macromolecules* **1974**, *7*, 698.
(17) Ramachandran, G. N.; Bansal, M. *Curr. Sci.* **1976**, *45*, 647.
(18) Rich, A.; Crick, F. H. C. *Nature (London)* **1955**, *176*, 915.
(19) Momany, F. A.; Carruthers, L. M.; McGuire, R. F.; Scheraga, H. A. *J. Phys. Chem.* **1974**, *78*, 1595.
(20) The role of this change of bond angle was tested by generating a triple-stranded $(GAP)_4$ complex in the conformation corresponding to the lowest energy structure[2] of $(GPP)_4$, using an artificial Ala residue, with $\tau(NC^{\alpha}C') = 111.0°$, as in proline. The repulsive interactions were reduced by the change in geometry.
(21) Madison, V. *Biopolymers* **1977**, *16*, 2671; **1979**, *18*, 1563.
(22) Némethy, G.; Scheraga, H. A., to be submitted for publication.
(23) Cowan, P. M.; McGavin, S. *Nature (London)* **1955**, *176*, 501.
(24) Brahmachari, S. K.; Ananthanarayanan, V. S. *Proc. Natl. Acad. Sci. U.S.A.* **1979**, *76*, 5119.
(25) Hopfinger, A. J.; Walton, A. G. *Biopolymers* **1970**, *9*, 29.

X-ray Diffraction Analysis of the Structure of Poly(dichlorophosphazene)[1]

H. R. Allcock,* R. A. Arcus, and E. G. Stroh

Department of Chemistry, The Pennsylvania State University, University Park, Pennsylvania 16802. *Received October 2, 1979*

ABSTRACT: Improved X-ray diffraction photographs, containing 63 unique reflections, have been obtained for highly purified poly(dichlorophosphazene) with the use of inclined-beam X-ray techniques. The results have been analyzed by a combination of unit cell indexing, model building, conformational analysis, and helical and optical transform methods. The chain-repeat distance is 4.92 Å. An exact structural solution was precluded by an unusual combination of factors that lead to disorder of the system. However, the data are consistent with a cis–trans planar chain conformation and with a chain-packing arrangement that allows appreciable "rotational" disorder between adjacent chains and additional disorder with respect to the directional "sense" of different chains. These factors help to explain the unusual physical properties of this polymer.

In this paper we explore the conformational and chain-packing structure of poly(dichlorophosphazene), $(NPCl_2)_n$ (I), by means of an analysis of X-ray diffraction data.

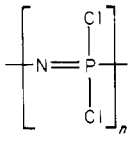

I

The objectives of this study were to obtain improved molecular structural data for this polymer and to correlate the unusual physical properties of this material with the molecular and chain-packing features. Poly(dichlorophosphazene) is one of the simplest polyphosphazenes known. As such, it provides a vital starting point for an understanding of the structural characteristics of the more complex poly(organophosphazenes).[2-12]

Two other high-polymeric phosphazenes have been investigated by X-ray diffraction techniques. The structure of the low-temperature form of poly(difluorophosphazene), $(NPF_2)_n$, was solved by Allcock, Kugel, and Stroh.[13] The organophosphazene poly[bis(*p*-chlorophenoxy)phosphazene] studied by Bishop and Hall,[14] but the structure proposed had a high discrepancy factor (45%). Chain repeat distance information was obtained by Allcock, Kugel, Valan, Siegel, and Stroh,[3,15] for the polymers $[NP(OCH_2CF_3)_2]_n$ and $[NP(OC_6H_5)_2]_n$, but difficulties were encountered in the complete structure solutions of these materials.

Poly(dichlorophosphazene) itself has been studied by earlier investigators. One of the earliest attempts to solve the structure of any polymer (inorganic or organic) was carried out in 1936 by Meyer, Lotmar, and Pankow[16] with a cross-linked form of $(NPCl_2)_n$. On the basis of an analysis

0024-9297/80/2213-0919$01.00/0

of only 22 reflections, they suggested the existence of a helical chain conformation with two monomer units per repeat distance of 4.92 Å. Three possible space groups were considered, $Pna2_1$, $Pnn2$, and $Pnnn$, with a later preference being mentioned[17] for $Pna2_1$. The suggested regular helical conformation was derived from the symmetry restrictions of the possible space groups, the chain-repeat distance, and an estimate of the length of a P–N single bond. No intensity analyses were reported.

A second X-ray analysis of $(NPCl_2)_n$ was reported by Giglio, Pompa, and Ripamonti in 1962.[18] They proposed a slightly distorted "cis–trans planar" chain conformation on the basis of an optical transform analysis of 38 reflections. Skeletal torsional angles of 156 and 14° (planar zigzag = 0°, 0°) were suggested. This conformation was quite different from the one suggested by the earlier study. However, the Giglio, Pompa, and Ripamonti model failed to provide a good match between the observed X-ray intensities and the optical transform for a substantial number of reflections.

Recent improvements in the technique for X-ray fiber studies developed in our laboratory[19] have allowed us to obtain X-ray photographs from poly(dichlorophosphazene) that contain 63 unique, indexable reflections. Moreover, the poly(dichlorophosphazene) used in this present work was purified extensively by multiple precipitations under strictly anhydrous conditions[1] and it was not cross-linked. The approach taken in this study included attempted unit cell indexing and space group selection as a prelude to structure factor calculations, helical and optical transform analysis of the X-ray data, and calculation of conformational energy surfaces and chain-packing energies.

The specific questions that were kept in mind throughout this study were as follows: (1) What are the bond angles and bond lengths in this polymer? (2) Does the polymer occupy a preferred chain conformation in the extended state at 25 °C? (3) To what degree are the macroscopic properties of the polymer determined by the intermolecular interactions?

Experimental Section

Collection of X-ray Diffraction Data. Except for the following details, the synthesis of $(NPCl_2)_n$, the preparation of the fibers, and the use of the X-ray cameras were as described elsewhere.[1,19] The stretched fibers used in this work had a diameter equal to or slightly less than 0.12 mm. This was the optimum size for absorption by Cu Kα radiation, as calculated from the linear absorption coefficients.[20] The fibers for indexing and intensity measurements were stretched to 10 times their original length. The X-ray photographs were obtained for stretched fibers at 20 °C. As discussed elsewhere,[1] the crystalline melting temperature for the tensioned polymer is >39 °C, whereas the unstretched polymer undergoes crystallite melting at −7.2 °C.

The shapes of the arcs on the upper layer lines were such that difficulties were experienced in the exact location of the layer lines. These discrepancies were avoided by the construction of a transparent overlay to define the reciprocal axial repeat distances calculated from the positions of the meridional reflections. Intensity data were collected with the use of multiple-film techniques. The stronger intensities were measured by using a scanning optical densitometer. The weaker intensities were estimated by visual comparison with a calibration step wedge. The usual corrections for Lorentz, polarization, multiplicity, and spot-shape effects were applied.

Optical Diffractometer. An optical diffractometer manufactured by R. B. Pullin & Co. Ltd., with a Ferranti He–Ne laser, was used to generate diffraction patterns from masks of several representative polymer models. The masks were prepared from a 4 × 5 in. opaque film with holes punched to represent atomic positions. Each mask represented 15 monomer residues in a single chain array. Of these, roughly 10 monomer residues were illuminated by the diffractometer. The area of each hole was in proportion to the atomic number of each atom. Atom coordinates for the projections were calculated by a computer program, plotted at a scale of 1 cm/Å, and transferred to the mask by means of a Pullin pantograph punch. Cylindrical averaging effects were produced from separate masks that represented 15° successive rotations about the helical axis, with the diffraction pattern being generated by multiple exposures on the diffractometer. The diffraction patterns were recorded on film with a 35-mm camera.

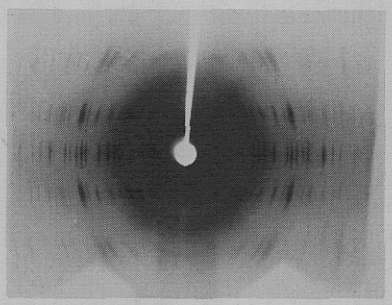

Figure 1. X-ray diffraction pattern of a highly stretched fiber of $(NPCl_2)_n$ obtained with Cu Kα radiation and a Weissenberg camera in the normal-beam geometry.

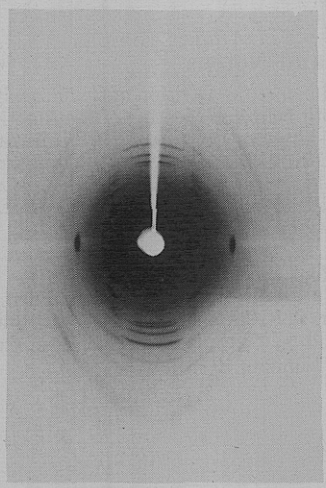

Figure 2. X-ray diffraction pattern of a highly stretched fiber of $(NPCl_2)_n$ with the fiber perpendicular to the fiber axis. A Weissenberg camera in the normal-beam geometry and Cu Kα radiation were used. The fiber was oscillated through 80° about the camera axis for an exposure time of 12 h.

Calculations. Calculations were carried out with an IBM 370/3033 computer at The Pennsylvania State University. Three programs, SFLS5A,[21] FORDAP,[22] and "Appleman",[23] were used. The Appleman program was used to refine unit cells and index reflections from the observed 2θ values and from initial trial unit cell parameters after graphical indexing had been carried out. The SFLS5A program was employed to generate structure factors for the unit cell models and for attempts to refine these models. The FORDAP program was used to generate two- and three-dimensional Patterson maps from the observed intensity data. The 13-atom conformational energy calculations were similar to those described previously,[24] but with the specific differences described in the text. A chain packing configuration program was written specifically for this study. The program was used to calculate energy maps for the unit cell packing arrangements derived from various chain conformations and packing configurations. The parameters for the Lennard-Jones and Coulombic calculations were obtained from the listing by Hopfinger,[25] as used previously.[24] Bessel function values[26] were used for the summations of the helical transform equations devised by Davies and Rich.[27]

Results and Discussion

Quality of the X-ray Diffraction Photographs. The X-ray diffraction patterns of oriented fibers of $(NPCl_2)_n$ showed excellent resolution of the individual reflections (Figures 1–3). Figure 4 shows a photograph with a resolution greater than 0.82 Å. This is probably the best

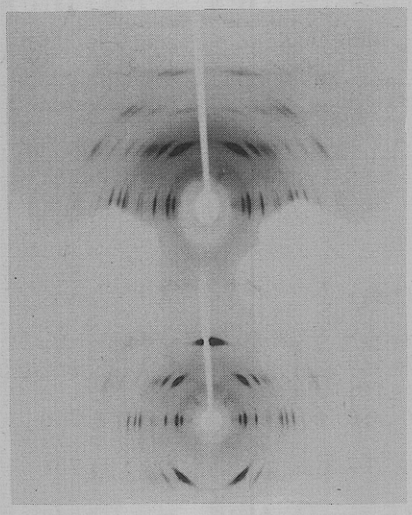

Figure 3. X-ray diffraction pattern of a highly stretched fiber of $(NPCl_2)_n$ obtained during a 3-h exposure with Cu Kα radiation and a Weissenberg camera in the flat-diffraction cone geometry for (a) the $l = 2$ layer line and (b) the $l = 1$ layer line.

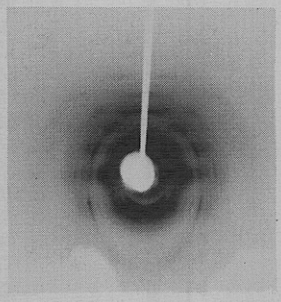

Figure 4. X-ray diffraction pattern of a highly stretched fiber of $(NPCl_2)_n$ obtained during a 3-h exposure with Mo Kα radiation and a Weissenberg camera in the flat-diffraction geometry for the $l = 3$ layer line.

resolution yet seen for the diffraction pattern of any polymer fiber. The use of equiinclination and flat-cone diffraction geometries[19] allowed the recording of upper level reflections not detected before for this polymer. Over 63 unique reflections were observed when Cu Kα radiation was used. The arcs were narrow in breadth, and reflections on the same layer line had the same shape. Calculations based on the arc lengths[28] showed that the crystallites were an average of 4° out of alignment with the fiber axis.

All the layer lines were of roughly the same intensity, which indicated that the atoms in the structure are distributed uniformly in the unit cell. The strong meridional reflection on the $l = 2$ layer line can be seen in Figures 2 and 3. The strongest reflections in the diffraction pattern appeared to represent genuine strong intensities rather than overlapping reflections. No back-scattering reflections were discernible above the background radiation fog. Attempts to induce double orientation in the polymer fiber had no effect on the diffraction pattern.

The high resolution of the X-ray photographs can be traced not only to the diffraction geometry employed but also to the mode of preparation of the polymer and the fibers. The best diffraction patterns were obtained from polymer that had the highest purity and had been prepared by a *low-conversion* polymerization of the cyclic trimer, $(NPCl_2)_3$. Thus, the polymer used in this work probably had a lower degree of interchain linkage and chain branching than the material used by earlier investigators. This, in turn, permitted greater degrees of fiber elongation and, ultimately, provided increased diffraction resolution. This is an important factor because, as discussed later, the resolution of the upper level reflections is a vital factor in the structure analysis of $(NPCl_2)_n$.

Polymer Repeat Distance and *d* Spacings. The crystallographic repeat distance is 4.92 Å. This value was determined from the separation of the layer lines of the diffraction patterns reproduced in Figures 1–4. This repeat distance remained constant as the temperature was varied from −110 to +39 °C. In addition, no conformational or phase changes were detected over this temperature range. The existence of a strong meridional reflection on the $l = 2$ layer line indicates that there are two monomer units per crystallographic repeat. An additional meridional reflection was observed on the $l = 6$ layer line, as shown in Figure 4. The observed d spacings and intensities are listed in Table I. These values were obtained from averaged measurements from the photographs reproduced in Figures 1 and 3.

Unit Cell and Space Group. In spite of the relatively large number of reflections detected, an unambiguous indexing arrangement could not be found. A large orthorhombic cell that contained four polymer chains was required in order to allow all the observed arcs to be indexed. However, use of the usual graphical[29] and analytical[30] methods for index assignment narrowed the choice to two plausible orthorhombic cells with similar dimensions. These cells will be designated here as orthorhombic-1 and orthorhombic-2.

The orthorhombic-1 cell was the "best-fit" unit cell derived by assignment of indices with the use of the least-squares routine of the Appleman program[23] and by a correlation of the observed and calculated 2θ values for each reflection, as shown in Table I. The cell constants were $a = 12.99 \pm 0.003$ Å, $b = 11.11 \pm 0.003$ Å, and $c = 4.92 \pm 0.002$ Å, with $V = 711$ Å^3. The calculated density, based on eight monomer residues per unit cell, is 2.16 g/mL. The observed density (by flotation) was 1.998 g/mL for a polymer that was 10–20% crystalline.[1] This unit cell was not ideal. A large number of the possible reflections had to be classified as "unobserved" rather than "missing" because of symmetry extinctions. Moreover, attempts to refine the molecular structure in space groups based on this cell were unsuccessful. The standard deviations for this cell were slightly better than those for the orthorhombic-2 cell.

The orthorhombic-2 cell was an A-centered cell derived by reassignment of reflections to account for missing reflections as genuine extinctions resulting from the centered symmetry. The cell parameters were refined by use of the Appleman program.[23] The cell constants for the orthorhombic-2 cell were $a = 13.01 \pm 0.02$ Å, $b = 11.09 \pm 0.02$ Å, and $c = 4.93 \pm 0.01$ Å, with $V = 713$ Å^3. The calculated density for eight monomer residues per cell is 2.15 g/mL. This type of unit cell would be compatible with a very high symmetry along individual chains and a highly symmetric packing arrangement.

The symmetry extinctions assigned to these two unit cells were not compatible with any specific space group.[31] The observed extinctions are listed in Table II. Several space groups with Laue symmetry *mmm* showed some correlation with the data, and these are shown in Table III.

Finally, attempts were made to determine the crystallographic symmetry by means of an analysis of plane groups and by Patterson image synthesis techniques. The five plane groups derived from the 001 projection of the 11 space groups are listed in Table III. Trial calculated structure factors derived from these plane groups showed a low correlation with the observed $hk0$ structure factors.

Table I
Observed *d* Spacings, Angles, and Structure Factors for $(NPCl_2)_n$ and Calculated *d* Spacings for Two Orthorhombic Unit Cells

	obsd values			calcd for orthorhombic-1 cell		calcd for orthorhombic-2 cell	
reflection no.	*d*, Å	θ, deg	F^a	*hkl*	*d*, Å	*hkl*	*d*, Å
1	6.491	6.821	25	200	6.494	200	6.504
2	5.545	7.991	48	020	5.553	020	5.547
3	4.220	10.52	25	220	4.221	220	4.221
4	3.410	13.07	12	320	3.415	320	3.416
5	3.251	13.72	20	400	3.247	400	3.252
6	2.801	15.94	27	420/330	2.803/2.81	420	2.806
7	2.716	16.49	44	140	2.715	140	2.713
8	2.543	17.65	43	240/510	2.553/2.530	240	2.551
9	2.352	19.13	49	520/340	2.353/2.337	520/340	2.355/2.330
10	2.111	21.42	26	440/250	2.110/2.101	440	2.110
11	1.852	24.60	40	060/700	1.851/1.856	060	1.849
12	1.779	25.68	26	260	1.780	260	1.779
13	1.704	26.91	25	360/640	1.702/1.707	360	1.701
14	1.628	28.27	14	800	1.624	800	1.626
15	1.559	29.65	25	820	1.558	820	1.560
16	1.401	33.38	52	840/920	1.402/1.397	840	1.403
17	1.320	35.75	13	380	1.322	380	1.321
18	1.261	37.68	12	10,2,0	1.265	10,2,0	1.266
19	1.176	40.98	12	10,4,0	1.177	10,4,0	1.178
20			0	001	4.92	001	4.93
21	3.716	11.97	53	211/021	3.702/3.687	211	3.707
22	3.147	14.18	32	311	3.122	311	3.127
23	2.889	15.48	24	131	2.886	131	2.887
24	2.726	16.43	21	401	2.712	231	2.694
25	2.655	16.88	21	411/231	2.634/2.694	411	2.638
26	2.474	18.16	15	331	2.444	331	2.445
27	2.258	20.05	36	511	2.251	511	2.253
28	1.972	23.01	47	601/531	1.982/1.953	531	1.954
29	1.813	25.17	10	351	1.835	351	1.834
30	1.741	26.28	86	701/631	1.737/1.747	631	1.749
31	1.570	29.41	9	731	1.572	731	1.574
32	1.522	30.44	15	811	1.528	811/071	1.530/1.560
33	1.492	31.12	13	821/171	1.486/1.500	171	1.499
34	1.380	33.97	24	911/901	1.374/1.385	911	1.376
35	1.297	36.48	11	931	1.297	931	1.299
36	1.240	38.44	10	941	1.239	671	1.239
37	2.460	18.26	16	002	2.460	002	2.465
38	2.231	20.21	23	122	2.220	122	2.223
39	1.969	23.05	35	402	1.963	402	1.967
40	1.870	24.35	6	332/422	1.854/1.851	422	1.854
41	1.795	25.43	33	502	1.788	242	1.774
42	1.712	26.76	70	522	1.702	522	1.704
43	1.575	29.31	15	622	1.561	622	1.563
44	1.490	31.15	8	632	1.489	062	1.480
45	1.420	32.56	28	722	1.432	722	1.434
46	1.361	34.49	15	802	1.356	802	1.358
47	1.316	35.85	18	822	1.317	833	1.319
48	1.213	39.45	53	922/082	1.215/1.210	082/922	1.209/1.217
49	1.149	42.13	11	10,0,2	1.149	10,0,2	1.151
50			0	003	1.643	003	1.643
51	1.586	29.08	26	203	1.593	213	1.580
52	1.531	30.23	17	223	1.531	313	1.525
53	1.454	32.02	23	413	1.454	413	1.456
54	1.385	33.81	41	243/503	1.382/1.389	513	1.380
55	1.310	36.06	17	603	1.309	153	1.315
56	1.245	38.27	61	543	1.242	353	1.236
57	1.225	39.00	39	453/163	1.223/1.223	713	1.225
58	1.162	41.58	8	733	1.167	733	1.169
59	1.124	43.31	9	273	1.124	273	1.125
60	1.232	38.74		004	1.230	004	1.210
61	1.213	39.46	20	204	1.211	204	1.213
62	1.149	42.14	20	234	1.151	404	1.154
63	1.108	44.09	14	514	1.108	244	1.111
64	0.820	70.07	15	006	0.820	006	0.821

[a] Values corrected for Lorentz, polarization, and spot-shape effects.

Two-dimensional Patterson maps of 001 projection were prepared, but the resolution was too low to resolve the space-group problem.

Three explanations seem plausible for the difficulties encountered in the assignment of a space group. First, it is conceivable that the unit cell is not orthorhombic. However, no other unit cells were found that provided a more satisfactory indexing scheme. A hexagonal cell was considered, mainly because the ratio d_{020}/d_{400} found for the orthorhombic cells (=1.71) was close to the ratio required for a hexagonal cell with $d_{100}/d_{120} = 1.732$,[32] but a satisfactory indexing could not be achieved. A primitive

Table II
Observed Extinction Rules for the Two Orthorhombic Unit Cells

Orthorhombic-1 Cell			
$0kl$:	$k + l = 2n + 1$	$h0l$:	$h = 2n + 1$
$0kl$:	$k = 2n + 1$	$h00$:	$h = 2n + 1$
$0kl$:	$l = 2n + 1$	$0k0$:	$k = 2n + 1$
$hk0$:	$k = 2n + 1$	$00l$:	$l = 2n + 1$
$h0l$:	$h + l = 2n + 1$		
Orthorhombic-2 Cell			
hkl:	$k + l = 2n + 1$	$h0l$:	$l = 2n + 1$
$0kl$:	$k + l = 2n + 1$	$hk0$:	$k = 2n + 1$
$0kl$:	$k = 2n + 1$	$h00$:	$h = 2n + 1$
$0kl$:	$l = 2n + 1$	$0k0$:	$k = 2n + 1$
$h0l$:	$h + l = 2n + 1$	$00l$:	$l = 2n + 1$
$h0l$:	$h = 2n + 1$		

Table III
Possible Space Groups for $(NPCl_2)_n$ Based on the Observed Extinctions

space group	International Tables desig	001 plane group[a]
Orthorhombic-1 Cell		
Pn2b (No. 30)	*Pnc2*	*p1m1*
Pnmb (No. 53)	*Pmna*	*p2mm*
Pnam (No. 62)	*Pnma*	*p2gg*
$Pna2_1$ (No. 33)	*Pna2*	*p2gg*
Pnab (No. 60)	*Pbcn*	*p2mg*
Pnnb (No. 52)	*Pnna*	*p2mg*
Orthorhombic-2 Cell		
Acam (No. 64)	*Cmca*	*p2mg*
Aba2 (No. 41)	*Aba2*	*p2mg*
Amam (No. 63)	*Cmcm*	*p2mg*
$A2_1am$ (No. 36)	$Cmc2_1$	*p1g1*
Ama2 (No. 40)	*Ama2*	*p2mg*

[a] The plane group that corresponds to the symmetry of the 001 projection of the space group listed.

monoclinic cell with $a = 13.01$ Å, $b = 6.07$ Å, $c = 4.93$ Å, and $\beta = 114°$, with $V = 356.5$ Å^3, showed some correlation with the experimental data, as did a triclinic cell with $a = 16.20$ Å, $b = 5.98$ Å, $c = 4.89$ Å, $\alpha = 68.28°$, $\beta = 53.24°$, and $\gamma = 77.33°$, but neither cell was completely compatible with the data. The triclinic cell, in particular, did not account for the meridional reflections.

Second, it is possible that multiple unit cells are present, with different packing configurations of the same repeat distance in different crystallites. An argument against this interpretation is that the overall intensity pattern of the X-ray photographs was not altered by changes in the mode of crystallization.[1]

Third, the crystallites may be "twinned" or statistically disordered. If so, an exact structural solution would be impossible unless the precise mode of disorder could be identified in such a way as to permit an assignment of the correct indices. Several experimental observations support the belief that the system is twinned or partly disordered. The unit cell of $(NPCl_2)_n$ is twice as large as the cell derived earlier[13] for $(NPF_2)_n$. Furthermore, the distribution of the intensities along each layer line shows sharp discontinuities, with the strongest reflections corresponding to a linear lattice (Figure 9). In addition, slight differences in the intensities of two reflections have been observed[1] in the diffraction patterns from $(NPCl_2)_n$ that has been crystallized by cooling or by elongation. This behavior could indicate a twinned or partly disordered lattice.

The Alternative Approach. In view of the difficulties encountered with the identification of a unique space group, it was not possible to solve the structure of $(NPCl_2)_n$ by standard structure factor techniques. Instead, an attempt was made to identify the molecular conformation of individual chains of $(NPCl_2)_n$ by a combination of helical transform calculations, optical transform analysis, and chain conformational energy calculations. Then, possible packing arrangements that such chains might assume in a microcrystalline lattice were explored. This approach requires the postulation of appropriate models for the single-chain structure, and the derivation of the models requires an estimate to be made of the bond angles, bond lengths, and accessible conformations. The bond-distance and bond-angle data were obtained from small-molecule structure results, and the accessible conformations of the chain were estimated from conformational energy surfaces.

Structural Values for the Polymeric Models. It seems clear from synthetic work,[1-12] NMR spectroscopy results, and the known structure of $(NPF_2)_n$[13] that $(NPCl_2)_n$ has an open-chain structure of the type shown in I. A large number of a single-crystal X-ray diffraction studies of small-molecule cyclic phosphazenes[5] have shown that the P–N bond distances do not alternate in length and that the geometry at phosphorus is that of a distorted tetrahedron with an N–P–N angle near 120° and an exocyclic Cl–P–Cl angle near 102°. For chlorocyclophosphazenes specifically, the values shown in Table IV have been reported.[33-36] The main variable in these structural parameters is the P–N–P bond angle, which is extremely flexible and can change within the range 121–159° to accommodate the restrictions of different-sized rings. Small variations have also been reported in the P–N bond distance and, within limits, these can be attributed to the bond contractions that accompany decreased steric strain with increased ring size. On the basis of the values listed in Table IV, the parameters for the $(NPCl_2)_n$ models were as follows: P–N = 1.52–1.60 Å, P–Cl = 1.96 Å, N–P–N = 119°, P–N–P = 125–160°, Cl–P–Cl = 102°.

Accessible Conformational States. It was first necessary to identify conformational states that are energetically feasible. This information, together with the restrictions imposed by the measured polymer repeat distance and the presence of the meridional reflections, was then used to identify plausible models for the single-chain analysis.

The first approach to this problem involved examination of space-filling molecular models of $(NPCl_2)_n$. This approach suggested that the least-hindered extended-chain conformation is cis–trans planar (0°, 180°) (Figure 5a). Such a conformation could generate the 2_1 helical structure required by the X-ray fiber diagram. An alternative possibility is a twisted trans–trans arrangement in which a chlorine on one phosphorus is interlocked tightly between

Table IV
Known Structural Parameters for Several Chlorocyclophosphazenes, $(NPCl_2)_x$

x	P-N, Å	P-Cl, Å	P-N-P, deg	N-P-N, deg	Cl-P-Cl, deg	ring conform	density, g/mL
3[33]	1.581	1.993	118.4	121.4	101.4	slightly puckered	1.99
4 (K)[34]	1.57	1.99	121	131	103	tub[a]	2.18
4 (T)[35]	1.56	1.99	121	134/138	103	chair	2.17
5[36]	1.521	1.961	118.4	148.6	102.2	close to planar	2.02

[a] The metastable form.

Table V
Internal Coordinates of Different Chain Models

model	P-N, Å	P-Cl, Å	N-P-N, deg	P-N-P, deg	Cl-P-Cl, deg	ψ,[a] deg	ϕ,[a] deg
A	1.60	1.96	120.0	125	102.0	180.0	0.0
B	1.60	1.99	119	127	103	156.0	14.0
C	1.60	1.96	120.0	133.5	102.0	75.5	75.5
D	1.60	1.96	120.0	105.7	102.0		−2.55
E	1.52	1.96	118.0	141.5	102.0	180.0	0.0
F	1.52	1.96	118.0	147.7	102.0	85.2	74.8
G	1.52	1.96	118.0	113.5	102.0		−2.63

[a] ψ and ϕ represent the torsional angles of two adjacent backbone bonds. 0°,0° corresponds to a trans-trans planar (planar zigzag) conformation.

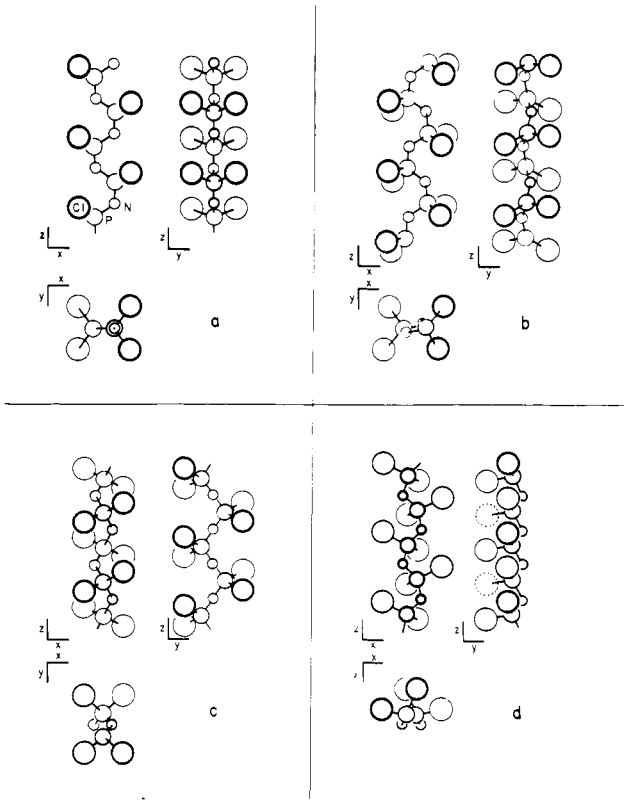

Figure 5. Projections of four models used for the calculation of helical transforms: (a) model A; (b) model B; (c) model C; (d) model D. The relative atomic dimensions shown are approximately half of the van der Waals radii.

the two chlorine atoms on the next phosphorus in an alternating arrangement. This structure is unusual because it orients all the chlorine atoms on one side of the backbone and all the nitrogen lone pairs on the other. It also generates a helix. However, the 4.92-Å repeat distance can be attained in this model only by a contraction of the P–N–P angle to the abnormally narrow value of 112–116°. Hence, this model was considered to be less plausible than the 0°, 180° structure. Later studies removed this conformation from consideration, largely because of the unusual bond angles required and the poor agreement with the intensity profile.

Nonbonding intramolecular potential energy calculations were then carried out for the extended-chain structures at, or slightly displaced from, the cis–trans planar conformation. Earlier calculations[24] performed without any restrictions imposed by a repeating array had also suggested that a near 0°, 180° conformation represented one of several acceptable arrangements. In the present work, similar calculations were performed with the restriction that each conformation generated by torsional displacement from the 0°, 180° starting point must generate a 2_1 helix.[37] Two approaches were explored. First, the polymer repeat distance was fixed at the experimentally measured value and the P–N bond distance and N–P–N angles were also kept constant. Thus, the variations in skeletal torsional angles induced a synchronous variation in the P–N–P bond angle. Second, the P–N bond distance and the N–P–N and P–N–P angles were kept constant as the skeletal bonds were allowed to undergo torsion. The P–N–P angle chosen was the value needed to generate the correct repeating distance for the cis–trans planar conformation (0°, 180°).[38] This approach caused a contraction in the calculated repeating distance as the torsional angles were changed from 0°, 180°.

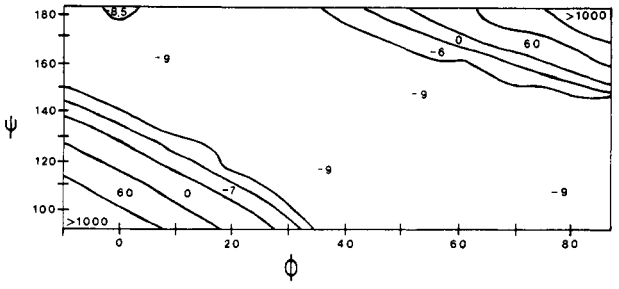

Figure 6. Energy surface for $(NPCl_2)_n$ in the region of ψ = 180°, ϕ = 0° (cis–trans planar conformation).

Both types of calculations suggested the existence of a broad, shallow minimum that encompassed a wide variety of conformations derived from the 0°, 180° conformer. In fact, the calculations showed no strong preference (<0.6 kcal/$NPCl_2$ unit) for any of the 2_1 helical arrangements within roughly 20° on either side of ψ_1 = 0° or ψ_2 = 180° or for any one of the three P–N bond lengths used (1.52, 1.54, 1.60 Å). Figure 6 shows the energy surface calculated for one particular set of structural parameters. The outer edges of this broad well are defined initially by the Cl···N repulsions.

Specific Conformational Models. Seven specific model structures were used to generate calculated transforms for comparison with the observed X-ray pattern. These models are described in Tables V and VI. Of these, two represent cis–trans planar arrangements (models A and E), one is a distorted cis–trans planar form (model B), two represent a "no-dipole" helix (models C and F), and two generate a twisted trans–trans conformation (models D and G). This set of models was chosen to provide a broad range of test data for comparison with the experimental X-ray pattern. As can be seen from Table V, the effects of bond-angle and bond-length changes for models A, C, and D are determined by comparisons with models E, F, and G, respectively. In all cases, the P–N–P bond angle was chosen to generate a chain-repeat distance of 4.92 Å once the other structural parameters had been defined.

Of these structures, model B represents the conformation proposed earlier by Giglio, Pompa, and Ripamonti.[18]

Table VI
Cartesian Coordinates of Different Chain Models[a]

model	atom	x	y	z
A	N_1	−0.638	0.000	0.000
	P_1	−0.710	0.000	1.598
	Cl_1	−1.805	1.523	2.166
	Cl_2	−1.805	−1.523	2.166
B[b]	N_1	0.570	0.251	1.572
	P_1	0.735	0.000	0.000
	Cl_1	1.752	1.503	−0.816
	Cl_2	2.015	−1.503	−0.248
C	N_1	0.637	0.000	0.000
	P_1	0.000	0.800	1.233
	Cl_1	1.360	2.033	0.530
	Cl_2	−1.360	2.033	1.930
D	N_1	−0.638	0.000	0.000
	N_2	0.638	0.000	2.460
	P_1	−0.336	0.705	1.404
	P_2	0.336	0.705	3.864
	Cl_1	0.339	2.512	1.054
	Cl_2	−2.045	1.072	2.291
	Cl_3	−0.339	2.512	3.514
	Cl_4	2.045	1.072	4.751
E	N_1	−0.430	0.000	0.000
	P_1	−0.739	0.000	1.488
	Cl_1	−1.904	1.523	1.895
	Cl_2	−1.904	−1.523	1.895
F	N_1	0.413	0.000	0.000
	P_1	0.000	0.783	1.233
	Cl_1	1.444	2.016	0.749
	Cl_2	−1.444	2.016	1.717
G	N_1	−0.430	0.000	0.000
	N_2	0.430	0.000	2.460
	P_1	−0.322	0.705	1.342
	P_2	0.322	0.705	3.802
	Cl_1	0.466	2.478	1.067
	Cl_2	−2.123	1.152	1.972
	Cl_3	−0.466	2.478	3.527
	Cl_4	2.123	1.152	4.432
H[b,c]	N	0.623	0.000	1.597
	P	0.725	0.000	0.000
	Cl_1	1.854	1.536	−0.572
	Cl_2	1.854	−1.536	−0.572
I[c,d]	N	0.623	0.000	1.597
	N_1	0.623	0.000	−2.169
	P	0.725	0.000	0.000
	P_1	0.725	0.000	−1.144
	Cl_1	1.854	1.536	−0.572
	Cl_2	1.854	−1.536	−0.572

[a] The Cartesian and internal coordinates of models C, D, F, and G were calculated by normal geometry. The transformation equations described by Miyazawa[39] were used to calculate cylindrical and Cartesian coordinates for models A, B, and E from selected internal coordinates and the fiber repeat distance. [b] Coordinates for the model first proposed by Giglio, Pompa, and Ripamonti.[18] [c] These models were used for the optical transform analysis only. [d] This model represents a "disordered" backbone arrangement of cis-trans planar chains in which different chains have the opposite directional "sense". The nitrogen and phosphorus atoms are assigned a one-half occupancy.

Models C and F were included because this general helical array is the only plausible conformation for $(NPCl_2)_n$ that generates no net dipole moment along the chain. Thus, this arrangement would not require the complementary presence of nearby chains to cancel the dipole in a crystal lattice. The twisted trans-trans conformation, mentioned earlier, is the only model in the set which is not a 2_1 helix. The monomer alternation feature of this structure is a glide plane rather than a twofold screw axis. Hence, extinctions of the type $l = 2n + 1$ would be expected. The dipoles for this structure would be contained in the glide plane. The difference between models D and G is largely one of different Cl···Cl contact distances for the "nested" chlorine (2.55 Å for model D and 2.63 Å for model G). Both of these values are less than the predicted sum of the van der Waals radii (3.6 Å).[39] Of all these possibilities, the cis-trans planar model is the most compact, has the highest symmetry, and can most easily accommodate the bond angles and bond lengths that are found in cyclic chlorophosphazene structures. The net dipole moment for this structure (and for distorted modifications of it) would be along the chain axis.

The *xy*, *xz*, and *yz* projections of models A–D are shown in Figure 5. The projections for models E–G would resemble the companion structure in those shown.

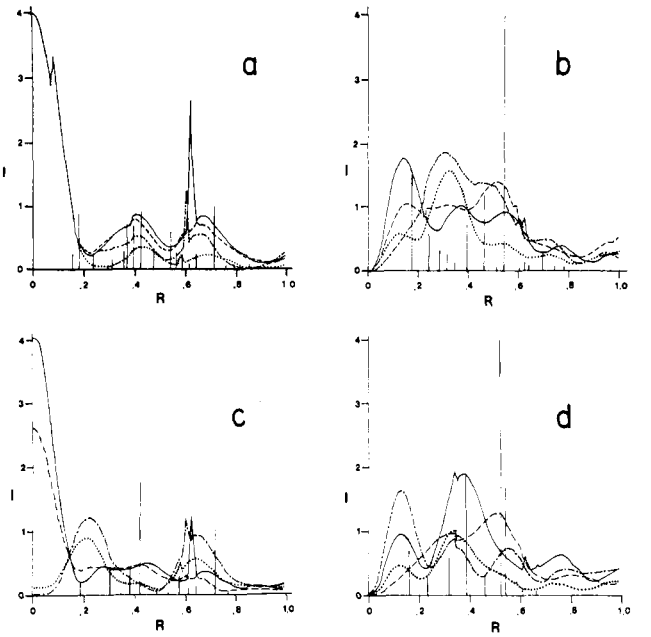

Figure 7. Calculated helical transform envelopes for different models for $(NPCl_2)_n$. The solid line is for model A, the dashed line is for model B, the alternating dash-and-dot line is for model C, and the dotted line is for model D. The vertical lines represent the observed intensities: (a) $l = 0$ layer line; (b) $l = 1$ layer line; (c) $l = 2$ layer line; (d) $l = 3$ layer line.

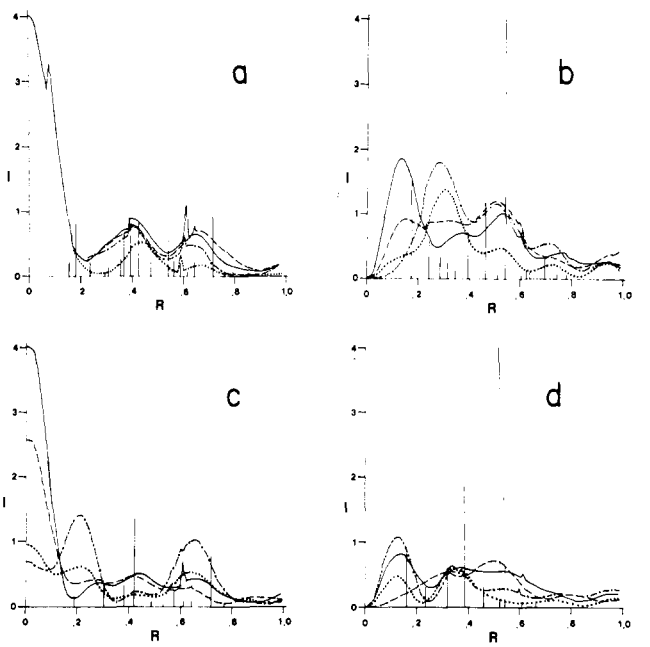

Figure 8. Calculated helical transform envelopes for model E (solid line), model B (dashed line), model F (alternating dash-and-dot line), and model G (dotted line). The vertical lines represent the experimentally observed intensities: (a) $l = 0$ layer line; (b) $l = 1$ layer line; (c) $l = 2$ layer line; (d) $l = 3$ layer line.

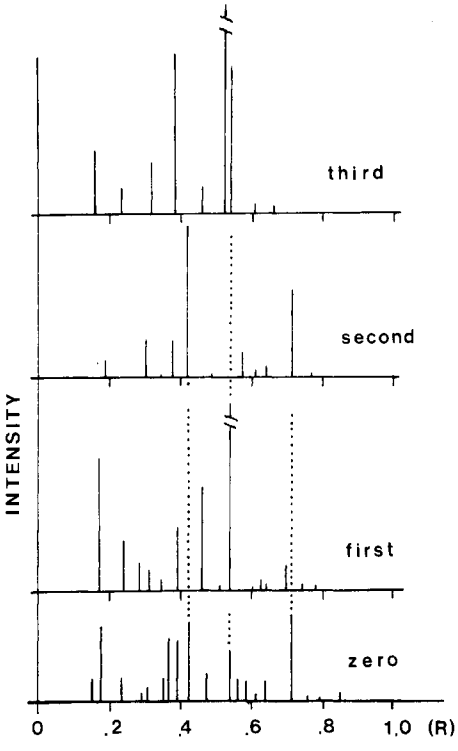

Figure 9. Comparison of the experimentally observed intensities on different layer lines.

Calculated Helical Transforms. The calculated helical transforms for layer lines $l = 0$ through $l = 3$ for models A–G are shown in Figures 7 and 8. The transforms shown in Figure 7 are for those models (A–D) that have the same P–N bond length (1.60 Å) and N–P–N angle (120°). In Figure 8 model B is compared with those models (E–G) that have the shorter P–N bond distance (1.52 Å) and narrower N–P–N angle (118°).

None of the calculated helical transforms provided an exact match for the observed intensities. The transforms for model E (a cis–trans planar conformation with a P–N bond distance of 1.52 Å) appeared to provide the best fit to the X-ray data. The worst fit was found for the "no-dipole" helical models (C, F).

The zero-level transforms were relatively insensitive to the conformational changes inherent in the different models. This is a consequence of the fact that the projection of the fiber repeat unit onto the xy plane is nearly the same for all of the models. This is shown in the xy projections in Figure 5. Thus, the differences between the various models can only be deduced by a comparison of the upper level calculated transforms with the observed X-ray intensities.

One of the unusual features of the observed X-ray intensity profile for $(NPCl_2)_n$ is the presence of very strong and very weak reflections with similar 2θ values on the same layer line. It is these very strong reflections that provide the greatest discrepancies with the calculated transforms. Figure 9 shows the relative observed intensities on different layer lines. A trend in the reciprocal radius values (R) of the strongest reflections is quite obvious. Most of the strong reflections that do not match any of the calculated transforms lie close to or on the linear reciprocal lattice of 0.178, 0.357, 0.536, and 0.714 $Å^{-1}$.

Optical Transform Analysis. Optical transforms were obtained from model B, described earlier, and for two additional cis–trans planar models, designated models H and I (see Tables V and VI). Model I differs from all the other structures examined with respect to the *orientation* of individual adjacent chains. As discussed earlier, the cis–trans planar conformation generates a directional "sense" to each chain. Model I allows different adjacent chains to possess an opposite "sense": the dipoles of the different chains are opposed. The zero-level transforms (the middle level of each photograph) were nearly indistinguishable for the three models. However, the details of the upper layer line profiles were different. The transform from model I showed a much better match to the X-ray diffraction pattern than does model B or H. In particular, model I predicts a meridional reflection on the $l = 6$ layer line, an ill-defined meridional reflection on the $l = 4$ layer line, and weak intensities on the $l = 5$ layer line, features that are evident in the X-ray photograph shown in Figure 4. The matching of the optical transform cross sections with the observed X-ray intensities for model I is shown in Figure 10.

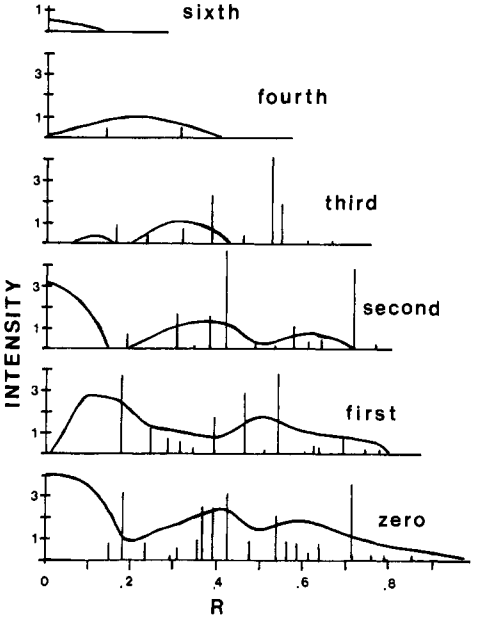

Figure 10. Optical transform envelopes calculated for model I compared with the experimentally observed intensities (vertical lines) for the $l = 0$ to $l = 6$ layer lines.

It is recognized that the failure to observe an exact match between the experimental and calculated data could result from the limited number of trial structures explored or a misestimate of the bond angles or bond lengths. However, for the reasons discussed in the next section, it was concluded that packing disorder constituted a far more serious source of discrepancy.

Chain-Packing Configurations. Exploratory calculations were carried out to deduce the chain-packing energies of cis–trans planar forms of $(NPCl_2)_n$ in various orthorhombic lattices. The calculations explored the influence on the intermolecular energy (derived from 6–12 Lennard-Jones potential, plus a Coulombic term) of the effects of (a) different numbers of chains oriented in a parallel fashion down the c axis of the unit cell, (b) independent axial rotation of separate chains in a given array, and (c) the adjacent packing of chains with an opposite directional "sense". Specifically, a chain model was used in which P–N = 1.56 Å, P–Cl = 1.96 Å, Cl–P–Cl = 102°, N–P–N = 119°, and P–N–P = 136°. Comparative energies were calculated for cells that contained 8 phosphorus, 8 nitrogen, and 16 chlorine atoms as part of 4 chains per cell. Because of the placement of the chains in the unit cell, the nonbonding interactions were between parts of 7 or 9 chains occupying the unit cell. The program was written in order to explore the variations in relative energy re-

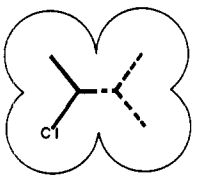

Figure 11. Cross-sectional projection of the van der Waals boundaries of $(NPCl_2)_n$ in the cis–trans planar conformation. The profile approaches circular symmetry.

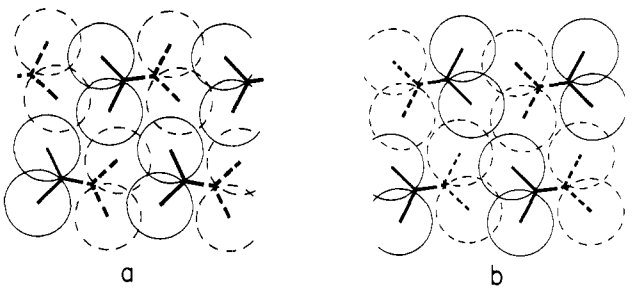

Figure 12. Two different plausible interchain packing arrangements for $(NPCl_2)_n$ in the cis–trans planar conformation. Individual chains are represented by a projection of two monomer residues approximately as viewed down the z axis.

sulting from independent rotation about the fiber axis of two different sets of nearby chains.

First, it was found that the cis–trans planar conformation of the chain generated lower energies than did the nonplanar conformations. For the cis–trans planar model the calculations showed quite clearly that a large number of potential packing arrangements would generate systems that were of comparably low energy. The van der Waals cross section of a cis–trans planar $(NPCl_2)_n$ chain approaches cylindrical symmetry (Figure 11). Therefore, the system can adopt may different interchain packing arrangements without a sacrifice in energy. Thus, disorder among discrete (cylindrical) orientations of adjacent chains and in the directional "sense" of each chain is to be expected. We believe that this accounts for the difficulties encountered in the assignment of this system to any one space group. An illustration of two different, but equally accessible, packing configurations is shown in Figure 12.

Conclusions

The X-ray diffraction evidence favors the existence of a cis–trans planar conformation of $(NPCl_2)_n$. This opinion is supported by the repeat distance of 4.92 Å, the location of the meridional reflections, the helical and optical transform experiments, and the chain-packing calculations.

The problems encountered in attempting to obtain an absolute structure solution can be traced to several factors that are almost unique to this polymer. First, the X-ray scattering ability of the $N–PCl_2$ unit is unusual for polymers. The scattering power of the backbone atoms is similar to the scattering power of the substituent atoms. Thus, the plane of greatest electron density is the triangle containing two chlorine atoms and a phosphorus and *not* the polymer chain axis. Thus, the normally simple task of locating the chain axis from the strongest reflections on the zero-layer line does not apply to this system. Moreover, no uniquely heavy atoms are present to assist in the phase assignments.

Second, it appears that the relative orientation of adjacent chains may be responsible for many of the puzzling features of the X-ray photographs. The ease with which axial reorientation of the chains can apparently occur and the possibility that chains with the opposite directional "sense" can pack together readily (Figure 13) to generate disorder appear to preclude a precise solution of this

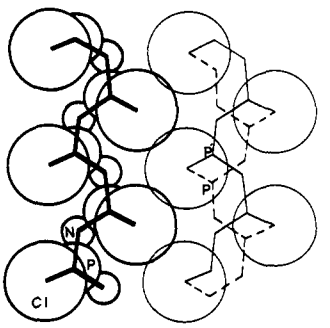

Figure 13. Presumed interchain packing arrangement for two adjacent chains of $(NPCl_2)_n$, demonstrating the ease of packing irrespective of the directional "sense" of each chain. In the structure seen on the right, the solid lines indicate the bond orientation for a chain with the same directional sense and the same atomic dispositions (P′) as the one seen on the left. The dashed broken line shows the orientation of bonds in a chain with the opposite directional sense. Although the atomic locations (P) do not mimic those seen in the structure on the left, the chlorine atoms do occupy the same relative position as in the adjacent structure. Hence, *chain* disorder appears likely even though disorder of the chlorine atoms may not be detected.

structure with the use of current techniques. Surprisingly, the prospect exists that the more complex poly(organophosphazene) structures may prove easier to solve than this simpler parent species.

Acknowledgment. The authors thank the Army Research Office for the support of this work and D. K. Smith, E. Ryba, R. S. Morgan, J. Reissner, and M. M Coleman for their comments and suggestions.

References and Notes

(1) For a related paper on the crystalline transitions and related physical properties of poly(dichlorophosphazene) see H. R. Allcock and R. A. Arcus, *Macromolecules*, **12**, 1130 (1979).
(2) H. R. Allcock and R. L. Kugel, *J. Am. Chem. Soc.*, **87**, 4216 (1965).
(3) H. R. Allcock, R. L. Kugel, and K. J. Valan, *Inorg. Chem.*, **5**, 1709 (1966).
(4) H. R. Allcock and R. L. Kugel, *Inorg. Chem.*, **5**, 1716 (1966).
(5) H. R. Allcock, "Phosphorus-Nitrogen Compounds", Academic Press, New York, 1972.
(6) H. R. Allcock, *Angew. Chem., Int. Ed. Engl.*, **16**, 147 (1977).
(7) J. E. White and R. E. Singler, *J. Polym. Sci., Chem.*, **15**, 1169 (1977).
(8) N. S. Schneider, C. R. Desper, R. E. Singler, M. N. Alexander, and P. L. Sagalyn, "Organometallic Polymers", C. E. Carraher, J. E. Sheats, and C. U. Pittman, Eds., Academic Press, New York, 1978.
(9) R. E. Singler, N. S. Schneider, and G. L. Hagnauer, *Polym. Eng. Sci.*, **15**, 321 (1975).
(10) D. P. Tate, *J. Polym. Sci., Polym. Symp.*, **48**, 33 (1974).
(11) G. Allen, C. J. Lewis, and S. M. Todd, *Polymer*, **11**, 31, 44 (1970).
(12) S. H. Rose, *J. Polym. Sci., Part B*, **6**, 837 (1968).
(13) H. R. Allcock, R. L. Kugel, and E. G. Stroh, *Inorg. Chem.*, **11**, 1120 (1972).
(14) S. M. Bishop and I. H. Hall, *Br. Polym. J.*, **6**, 193 (1974).
(15) H. R. Allcock and E. G. Stroh, unpublished results.
(16) K. H. Meyer, W. Lotmar, and G. W. Pankow, *Helv. Chim. Acta*, **19**, 930 (1936).
(17) K. H. Meyer, "Natural and Synthetic High Polymers", Interscience, New York, 1950, p 100.
(18) E. Giglio, F. Pompa, and A. Ripamonti, *J. Polym. Sci.*, **59**, 293 (1962).
(19) Inclined-beam X-ray techniques, such as the use of flat-cone or equiinclination geometries, offer a number of advantages for fiber diagram work with polymers that have short repeating distances. The flat-cone technique, used with a layer line screen, allows upper level reflections to be recorded with only minimal distortion of the intensities. The sharpness of the diffraction arcs obtained by inclined-beam methods allows more accurate measurements to be made of the distances between arcs. A more detailed description of these techniques

will be published later.
(20) "International Tables for X-Ray Crystallography", Vol. III, Kynoch Press, Birmingham, England, 1968, Section 3.2.
(21) C. T. Prewitt, SFLS5A, SUNY at Stony Brook, modified by M. J. Bennett and B. M. Foxman.
(22) A. Zalkin, FORDAP, Lawrence Berkeley Laboratory, University of California, modified by G. Hamilton and J. A. Ibers.
(23) D. E. Appleman, D. S. Handwerker, and H. T. Evans, Abstracts of the Annual Meeting of the American Crystallographic Association, 1963, pp 42-3.
(24) The conformational energy calculation method is described in detail in H. R. Allcock, R. W. Allen, and J. J. Meister, *Macromolecules*, **9**, 950 (1976). The potential used was a 6-12 Lennard-Jones potential together with a Coulombic term of the type $D_{ij} = (kQ_iQ_j)/(\epsilon r_{ij})$. The partial charges, Q, were +0.70 for phosphorus, -0.32 for nitrogen, and -0.19 for chlorine. No intrinsic backbone torsional potential was applied for the reasons discussed in the article referenced above.
(25) A. J. Hopfinger, "Conformational Properties of Macromolecules", Academic Press, New York, 1973, p 47.
(26) Staff of the Computation Library at Harvard, "The Annals of the Computation Laboratory at Harvard University; Tables of Bessel Functions", Vol. III-VI, Harvard University Press, Cambridge, Mass., 1947.
(27) D. R. Davies and A. Rich, *Acta Crystallogr.*, **12**, 97 (1959).
(28) M. Kakudo and N. Kasai, "X-Ray Diffraction by Polymers", Elsevier, New York, 1972.
(29) C. W. Bunn, "Chemical Crystallography", Oxford University Press, Oxford, 1961.
(30) M. J. Buerger, "X-Ray Crystallography", Wiley, New York, 1942.
(31) One example of the problems encountered is as follows. The meridional rule for a simple 2_1 helix for $(NPCl_2)_n$ ($l = 2n + 1$) can be consequence of a 2_1 screw axis ($00l$, $l = 2n + 1$) or a c glide plane ($0kl$, $l = 2n + 1$, or $h0l$, $l = 2n + 1$). The observed extinctions defined neither a space group nor possible locations of the polymer chain axis.
(32) P. H. Lindenmeyer and R. Hoseman, *J. Appl. Phys.*, **34**, 42 (1963).
(33) G. J. Bullen, *J. Chem. Soc. A*, 1450 (1971).
(34) R. Hazelkamp, T. Migchelson, and A. Vos, *Acta Crystallogr.*, **15**, 539 (1962).
(35) A. J. Wagner and A. Vos, *Acta Crystallogr., Sect. B*, **24**, 707 (1968).
(36) A. W. Schlueter and R. A. Jacobson, *J. Chem. Soc. A*, 2317 (1968).
(37) The equations for these calculations were derived from those reported by T. Miyazawa, *J. Polym. Sci.*, **55**, 215 (1961).
(38) The value of the P-N-P angle depended on the P-N bond distance. For example, for a P-N bond distance of 1.60 Å, the P-N-P angle was 125° (model A, Table V). For a P-N bond distance of 1.52 Å, the P-N-P angle was 141.5° (model E, Table V).
(39) A. Bondi, *J. Phys. Chem.*, **68**, 441 (1964).

Microstructural Characterization of Polypropylenes by High-Resolution Pyrolysis-Hydrogenation Glass Capillary Gas Chromatography

Yoshihiro Sugimura, Tamio Nagaya, and Shin Tsuge*

Department of Synthetic Chemistry, Faculty of Engineering, Nagoya University, Nagoya 464, Japan

Takeshi Murata and Tsunezo Takeda

Analytical Application Laboratory, Shimadzu Seisakusho Ltd., 1-Nishinokyo, Kuwabara-cho, Nakagyo-ku, Kyoto 604, Japan. *Received November 6, 1979*

ABSTRACT: High-resolution pyrograms of isotactic, syndiotactic, and atactic polypropylenes were obtained by pyrolysis-hydrogenation glass capillary gas chromatography. The assigned characteristic peaks on the pyrograms were interpreted in terms of the stereoregularity and the degree of chemical inversion for the monomer units along the polymer chains.

It is well-known that many physical properties of propylene (PP) are affected not only by the average molecular weight and the molecular weight distribution but also by the stereoregularity and the degree of the chemical inversion in the polymer chain. However, many arguments exist about the polymerization mechanism of olefins, even for Ziegler-Natta catalysts. This is largely responsible for the insufficient and sometimes imprecise information about the microstructures of the resulting polymers. The structural characterization of PP has been carried out most extensively by IR,[1-6] ^{1}H NMR,[7-9] and ^{13}C NMR[10-15] spectral studies. Although the existence of the irregular tail-to-tail linkages of the monomer units along the polymer chain was pointed out by Natta et al.[2] and Tosi et al.,[3] most of the spectroscopic studies were focused on the stereoregularity by asssuming the normal head-to-tail linkages. Recently, Doi et al.[16,17] successfully applied ^{13}C NMR for the elucidation of the chemical inversions in PP.

In addition to the spectroscopic work mentioned above, pyrolysis-gas chromatography (PGC) has been also demonstrated to be a simple, but powerful, technique for studying the microstructures of PP.[18-27] Noffz et al.[20] adopted PGC and used a 100-m-long capillary column to separate the degradation products from various PP's without any hydrogenation. They suggested that qualitative distinction of the PP's differing in the stereoregularity was possible from the resulting diastereomeric olefins. Tsuchiya et al.[22] studied the thermal degradation of PP and pointed out the existence of the irregular monomer placement from resulting 2-methyl-1-hexene.

Most of the other PGC work made use of in-line hydrogenation followed by pyrolysis, using H_2 as a carrier gas in order to convert the resulting degradation products into saturated hydrocarbons.[19,21,24,26] Seeger et al.[26] achieved fairly good separation of the diastereoisomeric products between the trimers and the heptamers and suggested the possibility of estimating the stereoregularity in PP semiquantitatively by comparison with standard PP samples. The resolution of the associated peaks appearing on the reported pyrograms, however, is not still sufficient for complete assignment of the characteristic products.

Recently, we[28,29] developed a method for obtaining high-resolution pyrograms of polymers in which a furnace-type pyrolyzer attached to a high-resolution glass capillary column is used. This technique, employing in-line hydrogenation of the resulting degradation products just before the separation column,[30] was successfully applied to characterization of polyethylenes and ethylene-α-olefin

0024-9297/80/2213-0928$01.00/0